

Raman spectra of neutron-irradiated and Al-doped MgB₂

D. Di Castro,¹ E. Cappelluti,^{2,3} M. Lavagnini,³ A. Sacchetti,¹ A. Palenzona,⁴ M. Putti,⁴ and P. Postorino¹

¹*Coherentia-INFN-CNR and Physics Department, University of Rome "La Sapienza," Piazzale A. Moro 5, I-00185, Rome, Italy*

²*SMC-Institute for Complex System, INFN-CNR, Via dei Taurini 19, 00185 Rome, Italy*

³*Physics Department, University of Rome "La Sapienza," P.le A. Moro 5, I-00185, Rome, Italy*

⁴*Dipartimento di Fisica, INFN-LAMIA, Via Dodecaneso 33, 16146 Genova, Italy*

(Received 14 February 2006; revised manuscript received 28 August 2006; published 20 September 2006)

We carried out Raman measurements on neutron-irradiated and Al-doped MgB₂ samples. The Raman spectrum changes substantially in both cases and in a similar way, with the appearance of high-frequency spectral structures, whose spectral weight increases with increasing Al concentration and neutron irradiation fluence. In particular, in Al-doped samples the high-frequency peaks slightly harden with increasing Al concentration, due to the lattice compression, whereas in the neutron-irradiated samples, where no atomic substitution occurs, no frequency shift is detected. The appearance of high-frequency spectral structures in the irradiated samples, similar to those observed in Al-doped ones, is quite unexpected. By direct comparison of the Raman spectra with literature experimental phonon densities of states, we show that the modifications of the Raman spectrum in both irradiated and Al-doped samples are due to disorder-induced violations of the Raman selection rules. Theoretical calculations of the phonon density of states support this hypothesis, and demonstrate that the high-frequency structures arise mostly from contributions at $\mathbf{q} \neq \mathbf{0}$ of the E_{2g} phonon mode.

DOI: 10.1103/PhysRevB.74.100505

PACS number(s): 74.70.Ad, 63.20.Dj, 78.30.-j

A few years after the discovery of superconductivity in MgB₂, many of its characteristic properties have been investigated and mostly clarified. Nowadays a wide consensus exists about MgB₂ being a phonon-mediated two-gap, two-band superconductor,¹⁻⁵ where superconductivity mainly arises from the coupling of the holes in the σ band with the E_{2g} phonon mode, which involves the in-plane stretching vibrations of boron atoms.^{6,8-10} In order to identify the fundamental mechanisms of the superconducting pairing, a key role has been played by a variety of experimental techniques that permitted the tuning of the electronic and lattice properties of MgB₂, such as the application of external pressure,^{11,12} irradiation-induced disorder,¹³⁻¹⁵ chemical substitution (e.g., Al on the Mg site,^{16,17} and C on the B site^{18,19}). In many of these cases, a reduction of the critical temperature, or even a suppression of the superconducting phase, has been observed. In doped MgB₂ compounds, in particular, the debate focuses on the relevance and the relative weight of two different microscopic mechanisms responsible for the reduction of T_c , namely, the band filling effects that tune the electron density of states²⁰⁻²² and the disorder-induced increase of the interband scattering.^{7,23}

Since the early investigations on MgB₂, Raman spectroscopy has been widely applied because the doubly degenerate E_{2g} mode, responsible for superconductivity, is the only Raman-active mode among the four optical phonons (A_{2u} , B_{1g} , E_{1u} , and E_{2g}).^{10,24} Indeed, the most prominent feature of the measured Raman spectrum, namely, the very broad peak (width ~ 300 cm⁻¹) centered at around 620 cm⁻¹,^{11,24-26} has been generally identified with the E_{2g} phonon peak, whose predicted frequency at the zone center Γ lies within the 510–660 cm⁻¹ range.^{6,27} Despite the almost general consensus on the above assignment, however, some controversial issues remain open,^{24,28,29} in particular regarding the anomalously large phonon linewidth and its remarkable temperature dependence.^{24-26,30} Different mechanisms, based on the strong electron-phonon (e -ph) coupling and on anharmonic effects, have been invoked to explain these

features,^{11,25,26,31,32} although recent theoretical calculations suggest that these effects do not fully account for the experimental findings.²⁹ As an alternative idea, the anomalously large line shape was proposed to be related to the excitations of phonons outside the Γ point activated by lattice defects and multiphonon scattering.²⁹ This hypothesis has also been suggested by some experimental works where the large phonon line shape,²⁸ and other weak spectral features in the Raman spectrum,²⁵ were ascribed to phonon contributions, throughout the Brillouin zone, activated by disorder-induced relaxation of the Raman selection rules.

Raman experiments have been also carried out on pure and doped MgB₂ films³²⁻³⁴ and on bulk chemically substituted MgB₂ compounds.^{17-19,25} Also, in these cases, the attempts at a quantitative analysis lead to ambiguous and sometime contradictory results. Contrary to the prediction of one Raman-active mode only, the introduction of even small quantities of substitutional impurities appears to drive the onset of additional high-frequency (HF) structures around 750 and 850 cm⁻¹,^{17,19,25} which are absent or vanishingly small in the pure compound. At higher levels of substitution, the Raman signal becomes further complicated, progressively approaching the spectrum of the end compound. In Mg_{1-x}Al_xB₂ a two-step behavior is observed: the HF structures are well detectable at $x=0.05$ and, up to $x=0.25$, their intensity increases while keeping almost constant the frequency positions; for $x>0.25$ the intensities keep growing but the frequencies increase and the line shapes narrow, evolving as a whole toward the spectrum of the parent compound AlB₂.^{17,25} However, since C and Al doping induces, at the same time, charge doping, volume compression, and on-site lattice disorder, it is particularly difficult to disentangle their effects on the Raman spectrum and on the superconducting properties.

The present paper aims to single out the effect of the lattice disorder by carrying out a Raman study of differently neutron-irradiated MgB₂ samples.¹⁵ We show that neutron irradiation causes the appearance of HF spectral structures,

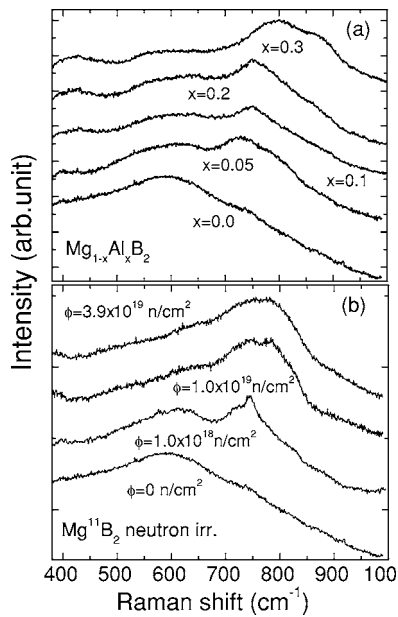


FIG. 1. Background-subtracted Raman spectra of Al-doped (a) and neutron-irradiated (b) MgB_2 samples. Spectra are shifted upward by a constant value.

similar to those observed in lightly Al-doped samples. The comparison of the present spectra with the literature data allows us to ascribe the unexpected HF Raman features, present in the irradiated and lightly Al-doped sample, to a disorder-induced violation of the Raman selection rules. Theoretical calculations of the phonon dispersion curves support this hypothesis and allow us to compare the Raman results with differently \mathbf{q} -integrated phonon density of states (PDOS).

Isotopically enriched (^{11}B) polycrystalline MgB_2 was prepared by direct synthesis from pure elements.¹⁵ Three identical samples were irradiated by means of thermal neutrons at the source SINQ (Paul Scherrer Institut, Switzerland).¹⁵ Different irradiation times were applied to the samples to accomplish 7.6×10^{17} , 1.0×10^{19} , and 3.9×10^{19} n/cm^2 . The most important damage mechanism in our samples is driven by the neutron capture reactions by the residual amount of ^{10}B present (less than 0.5%). Lattice defects are created by the recoil of ^4He and ^7Li , produced by the nuclear reaction, which are emitted isotropically. This makes the defect distribution very homogeneous. After the irradiation, the resistivity progressively increases (16, 64, and 124 $\mu\Omega$ cm) and T_c decreases (35.9, 24.3, and 12.2 K) on increasing the fluence. For the sake of comparison the low Al-doped samples (5%, 10%, 20%, and 30% with a T_c of 36.6, 33.4, 29.1, and 24.1 K) were also prepared following a similar procedure.³⁵

Raman spectra were measured in backscattering geometry, using a confocal micro-Raman spectrometer equipped with a charge-coupled-device detector and notch filter to reject the elastically scattered light. The sample was excited by the 632.8 nm line of a 30 mW He-Ne laser. Raman spectra were collected using a $20\times$ objective (laser spot about $10 \mu\text{m}^2$ wide at the sample surface) over the frequency range $200\text{--}1100 \text{ cm}^{-1}$, which includes the whole phonon spectral region. For each sample Raman spectra were collected from

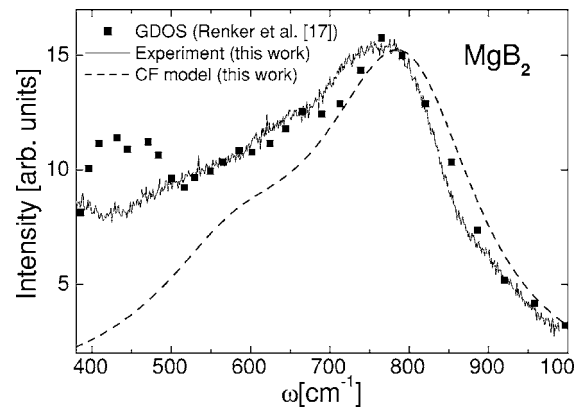


FIG. 2. Raman spectrum of the most irradiated sample (full line) compared with the PDOS from the neutron experiment of Ref. 17 (squares) and with the calculated E_{2g} -projected PDOS (dashed line). All the reported quantities are normalized to the same peak intensity.

different points on the sample surface and then averaged to avoid possible effects of preferred microcrystalline orientation.

The Raman spectra of the irradiated and Al-doped samples are shown in Fig. 1. Accordingly to literature data,^{17,25} the effect of Al doping on the Raman signal is that of driving the onset of a HF spectral structure. The Raman spectra of the irradiated samples, also shown in Fig. 1, present an unexpectedly strong dependence on the fluence. Quite interestingly, the two series are surprisingly similar: in both cases, HF structures appear and become dominant at the highest values of Al doping or neutron fluence. The same features, occurring at about the same frequencies, have been observed also in light C-doped MgB_2 ,^{19,32} and disordered films.³³ Since neutron irradiation has the *only* effect of disordering the lattice, these results suggest that the HF structures in the chemically substituted samples are produced mainly by the lattice disorder as well. In this context, the weak hardening of the frequencies of the HF structures, well detectable for only 30% Al-doped samples, could be likely ascribed to the Al-driven lattice compression.

The comparison between the Raman data in Al-doped compounds and in neutron-irradiated compounds gives rise to some fundamental questions, in particular concerning the origin of the HF structure and the role of the lattice disorder to make them visible. Most importantly, one could question whether the $\mathbf{q}=\mathbf{0}$ E_{2g} phonon mode is actually the only mode really probed in the Al-doped and irradiated samples. As we are going to discuss, we believe that the answer to the last question is negative and that we are actually probing some kind of phonon density of states.

In Fig. 2 the Raman spectrum of the highest irradiated sample is compared with the PDOS of MgB_2 measured by inelastic neutron scattering.¹⁷ Since no selection rules apply to neutron scattering, the excellent agreement between the experimental data over a wide frequency range ($500\text{--}1000 \text{ cm}^{-1}$) suggests that in disordered MgB_2 the Raman selection rules are notably relaxed and the Raman spectrum basically reflects the PDOS. On the other side, the apparent disagreement below 500 cm^{-1} suggests a remarkably

TABLE I. Force-constant parameters reproducing the bare phonon dispersion in MgB_2 in the absence of electron-phonon interaction.

| ϕ_r (eV/Å ²) | ϕ_{\parallel} (eV/Å ²) | ϕ_{\perp} (eV/Å ²) |
|---------------------------------|---|---------------------------------------|
| 12.45 | 49.80 | 21.17 |
| χ_r (eV/Å ²) | χ_{\parallel} (eV/Å ²) | χ_{\perp} (eV/Å ²) |
| 0.0 | 16.6 | 0.0 |
| κ_r (eV/Å ²) | κ_{\parallel} (eV/Å ²) | κ_{\perp} (eV/Å ²) |
| 0.84 | 1.50 | 9.14 |
| ψ_r (eV/Å ²) | ψ_{\parallel} (eV/Å ²) | ψ_{\perp} (eV/Å ²) |
| 0.0 | 9.34 | 0.42 |

different weight of the phonon modes in the Raman and the neutron experiment. In the present case we can assume that the lattice disorder, induced by neutron irradiation or by chemical substitution, mostly tunes the violation of the Raman momentum selection rules but not of the eigenvector selection.

For a more quantitative check of this empirical hypothesis, we calculated the phonon dispersion of MgB_2 within a force-constant (FC) shell model. Four elastic springs ϕ , χ , κ , and ψ , connecting, respectively, in-plane B-B nearest neighbors, out-of-plane B-B nearest neighbors, out-of-plane B-Mg nearest neighbors, and in-plane Mg-Mg nearest neighbors, are considered. Each elastic spring is specified by its tensor components (e.g., ϕ_r , ϕ_{\parallel} , ϕ_{\perp}), corresponding, respectively, to the lattice displacements along the radial (bond-stretching) direction and along the in-plane and out-of-plane tangential (bond-bending) directions. We set the values of the 12 parameters³⁶ by fitting the local-density functional phonon dispersion of Ref. 26 along the high-symmetry points of the Brillouin zone. Since the constant-force model is meant to reproduce the bare phonon dispersion, we deliberately did not include in the fitting procedure the E_{2g} phonon frequencies at the zone center Γ , A , which are known to be strongly affected by the e -ph interaction. The elastic constants so obtained are reported in Table I. The effects of the e -ph interaction involving the E_{2g} boron mode with the electronic σ band were included through the self-energy renormalization of the phonon frequencies,³⁶ $\Omega_{E_{2g}}^2(\mathbf{q}) = \omega_{E_{2g}}^2(\mathbf{q}) - (4N_{\sigma}g^2f_{\text{anharm}}/M_B)\Pi_{2D}(\mathbf{q})$, where N_{σ} is the density of states of the σ bands per spin and per band, g the electron-phonon matrix element between σ band electrons and the E_{2g} phonon mode at the zone center, and f_{anharm} is a dimensionless factor accounting for the anharmonic hardening of the E_{2g} phonon modes due to the electron-phonon coupling itself. Moreover the factor 4 takes into account the spin and band degeneracy and $\Pi_{2D}(\mathbf{q})$ is the two-dimensional Lindhardt function $\Pi_{2D}(x) = \theta(1-x) + \theta(x-1)(x - \sqrt{x^2-1})/x^4$, with $x = |\mathbf{q}|/2k_F$. We take, from first-principles calculations,^{8,10,37} $f_{\text{anharm}} = 1.25$, $N_{\sigma} = 0.075$ states/(eV spin cell), $g = 12$ eV/Å, and $k_F \approx \pi/12d_{\text{B-B}}$, where $d_{\text{B-B}}$ is the boron-boron distance.

In Fig. 3 we show the calculated phonon dispersion

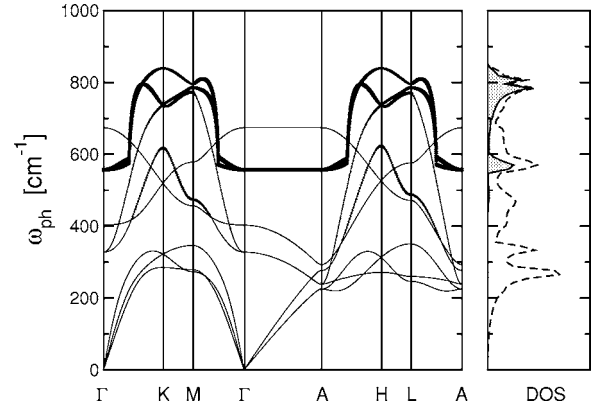


FIG. 3. Left panel: phonon dispersion of MgB_2 within the FC model. The thickness of the lines in the phonon dispersion reflects the magnitude of the E_{2g} component for each mode. Right panel: the corresponding total PDOS (dashed line), and the E_{2g} -projected PDOS (shaded area).

curves $\omega_{\mathbf{q},\mu}$ calculated in this way for the different phonon branches μ and the total PDOS (dashed line). Our calculations enable us to evaluate the eigenvectors of each phonon mode, and hence, in particular, their “ E_{2g} component” $\eta_{\mathbf{q},\mu}^{E_{2g}}$, which we believe to be effectively probed in our Raman measurements, by simply projecting the generic phonon eigenvector $\hat{\epsilon}_{\mathbf{q},\mu}$ on the E_{2g} one, $\hat{\epsilon}_{E_{2g}}$, $\eta_{\mathbf{q},\mu}^{E_{2g}} = |\hat{\epsilon}_{\mathbf{q},\mu} \cdot \hat{\epsilon}_{E_{2g}}|^2$. Thus, in Fig. 3 we show also the E_{2g} character of each phonon branch, as quantified by the thickness of the lines, as well as the “ E_{2g} -projected” phonon density of states (E_{2g} -PDOS), shown as the shaded area in the right panel, that is, the total PDOS weighted by the E_{2g} component $\eta_{\mathbf{q},\mu}^{E_{2g}}$. The resulting E_{2g} -PDOS, smeared by a Lorentzian function with width $\Gamma = 100$ cm^{-1} , to simulate the finite phonon lifetime, is also shown in Fig. 2 for comparison purposes. The good agreement between the E_{2g} -PDOS and the Raman spectrum of the highest irradiated sample supports the idea that the lattice disorder induces a violation of the Raman momentum selection rules, so that the effective spectra correspond to \mathbf{q} -integrated quantities. The slight difference on the low-frequency side could be ascribed to secondary contributions, disorder activated, from other Raman nonactive modes, such as the B_{1g} . It is also worth noticing that the peak in the PDOS at about 580–600 cm^{-1} and the HF structures at ~ 800 cm^{-1} ,

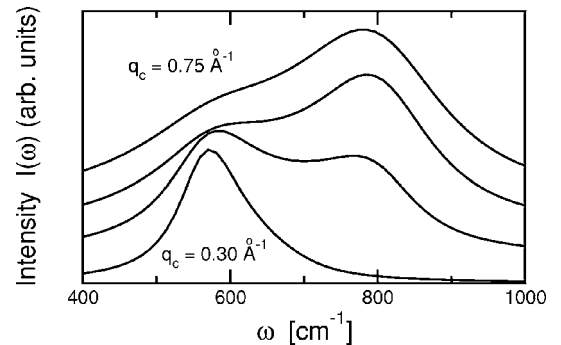


FIG. 4. Raman intensity from Eqs. (1) for different values of the cutoff q_c : (from the bottom to the top) $q_c = 0.30, 0.45, 0.60, 0.75$ Å⁻¹. Curves are shifted upward for clarity.

shown in Fig. 3, arise from the contribution of different regions of the Brillouin zone, respectively, from the \mathbf{q} states close to Γ -A and to K-M.

This observation suggests that the onset of the HF structures in the disordered samples could reflect the tuning of the breakdown of the momentum selection rules as induced by the amount of disorder. In simple terms, we argue that the momentum space effectively probed by the Raman measurements is steadily increased as the disorder itself is increased, so that only the $\mathbf{q}=\mathbf{0}$ E_{2g} phonon frequency at ~ 500 cm^{-1} is essentially probed in pure MgB_2 , while the total \mathbf{q} -integrated PDOS is probed in highly disordered samples. Varying the amount of disorder (with chemical doping or neutron irradiation) would thus tune the systems between these two extreme limits. In order to simulate this effect we model the Raman intensity by

$$I(\omega) = \frac{1}{N_c} \sum_{|\mathbf{q}| \leq q_c, \mu} \eta_{\mathbf{q}, \mu}^{E_{2g}} \frac{1}{\pi} \frac{\Gamma_{q_c}}{(\omega - \omega_{\mathbf{q}, \mu})^2 + \Gamma_{q_c}^2}, \quad (1)$$

where N_c is the number of sampling points in the Brillouin zone and where q_c is a momentum cutoff that takes into account the degrading of the \mathbf{q} -selection rules and that depends on the amount of disorder. In physical terms, q_c can be considered a measurement of the breakdown of the translational invariance induced by the disorder. We explicitly included in Eq. (1) also the presence of a finite phonon scattering rate Γ . On physical grounds, we expect that the phonon scattering rate Γ_{q_c} is also highly sensitive to the amount of disorder, here parametrized by q_c , with Γ_{q_c} increasing with increasing q_c . To take into account these effects we assumed a linear dependence on q_c , namely, $\Gamma_{q_c} = \alpha q_c$, where $\alpha = 120$ $\text{\AA}/\text{cm}^{-1}$.

In Fig. 4 we show the intensities calculated using Eq. (1) for different values of q_c (0.30, 0.45, 0.60, 0.75 \AA^{-1}). For $|\mathbf{q}| \leq 0.3$ \AA^{-1} we are essentially probing only the flat dispersion region close to the Γ point shown in Fig. 3, and only the low-energy structure at ~ 600 cm^{-1} is visible. However, for larger q_c the loss of the momentum selection rules

is strong enough to cause probing also of the $|\mathbf{q}|$ states close to the M and K points (we recall that $|\mathbf{q}_M| = 0.39$ \AA^{-1} and $|\mathbf{q}_K| = 0.68$ \AA^{-1}), making the HF structure of the E_{2g} -PDOS of Fig. 3 rapidly visible. Finally, for q_c larger than the size of the Brillouin zone, all the $|\mathbf{q}|$ states are equally probed, and the signal $I(\omega)$ approaches the full E_{2g} -PDOS (Fig. 2). The direct experimental vs theoretical comparison in Fig. 2, together with the remarkably similar trend shown by the spectra in Fig. 1 and the calculated intensities in Fig. 4, reveal that, also in disordered systems, the Raman spectrum mostly originates from the E_{2g} phonon branch. Giving the key role of the E_{2g} mode, this finding explains the frequently observed correlation between the Raman signal and the superconducting properties of MgB_2 -based compounds.^{17,19,25,32,33}

In conclusion, in this work we presented Raman spectra from differently neutron irradiated and Al-doped MgB_2 samples. We have shown that, on increasing the neutron irradiation dose (i.e., lattice disorder) as well as Al doping (i.e., point defects plus charge doping), HF structures appear and rapidly become the dominant spectral features. The remarkable similarity among our spectra and those reported in literature from lightly C-doped samples suggests that the lattice disorder, which is unavoidably present in the chemically substituted as well as in the irradiated sample, is mostly responsible for the modifications of the Raman signal. This is confirmed by the direct comparison between the Raman spectrum of the most irradiated sample and the neutron PDOS.¹⁷ We also showed that the loss of the Raman momentum selection rules, tuned by the amount of lattice disorder, can explain in a natural way the onset of the HF structures. Thus the present results provide a clear and unambiguous explanation of the Raman spectra in MgB_2 and address Raman spectroscopy as a very sensitive technique to investigate the role of lattice disorder in MgB_2 and, more in general, in systems where a strong coupling between the lattice and the electronic degrees of freedom exists. These findings also shed light on the interpretation of the previously reported Raman spectra in MgB_2 -based compounds.

¹S. L. Budko *et al.*, Phys. Rev. Lett. **86**, 1877 (2001).

²R. S. Gonnelli *et al.*, Phys. Rev. Lett. **89**, 247004 (2002).

³S. Souma *et al.*, Nature (London) **423**, 65 (2003).

⁴A. Y. Liu *et al.*, Phys. Rev. Lett. **87**, 087005 (2001).

⁵H. J. Choi *et al.*, Nature (London) **418**, 758 (2002).

⁶J. Kortus *et al.*, Phys. Rev. Lett. **86**, 4656 (2001).

⁷M. Monni *et al.*, Phys. Rev. B **73**, 214508 (2006).

⁸J. M. An and W. E. Pickett, Phys. Rev. Lett. **86**, 4366 (2001).

⁹Y. Kong *et al.*, Phys. Rev. B **64**, 020501(R) (2001).

¹⁰T. Yildirim *et al.*, Phys. Rev. Lett. **87**, 037001 (2001).

¹¹A. F. Goncharov *et al.*, Phys. Rev. B **64**, 100509(R) (2001).

¹²D. Di Castro *et al.*, Phys. Rev. B **72**, 094504 (2005).

¹³Y. Bugoslavsky *et al.*, Nature (London) **411**, 561 (2001).

¹⁴M. Eisterer *et al.*, Semicond. Sci. Technol. **15**, L9 (2002).

¹⁵M. Putti *et al.*, Appl. Phys. Lett. **86**, 112503 (2005).

¹⁶D. Di Castro *et al.*, Europhys. Lett. **58**, 278 (2002).

¹⁷B. Renker *et al.*, Phys. Rev. Lett. **88**, 067001 (2002).

¹⁸T. Masui *et al.*, Phys. Rev. B **70**, 024504 (2004).

¹⁹J. Arvanitidis *et al.*, J. Phys. Chem. Solids **65**, 73 (2004).

²⁰O. de la Pena *et al.*, Phys. Rev. B **66**, 012511 (2002).

²¹G. Profeta *et al.*, Phys. Rev. B **68**, 144508 (2003).

²²J. Kortus *et al.*, Phys. Rev. Lett. **94**, 027002 (2005).

²³S. C. Erwin and I. I. Mazin, Phys. Rev. B **68**, 132505 (2003).

²⁴K. Kunc *et al.*, J. Phys.: Condens. Matter **13**, 9945 (2001).

²⁵P. Postorino *et al.*, Phys. Rev. B **65**, 020507(R) (2001).

²⁶K. P. Bohnen *et al.*, Phys. Rev. Lett. **86**, 5771 (2001).

²⁷G. Satta *et al.*, Phys. Rev. B **64**, 104507 (2001).

²⁸X. K. Chen *et al.*, Phys. Rev. Lett. **87**, 157002 (2001).

²⁹M. Calandra and F. Mauri, Phys. Rev. B **71**, 064501 (2005).

³⁰H. Martinho *et al.*, Solid State Commun. **125**, 499 (2003).

³¹E. Cappelluti, Phys. Rev. B **73**, 140505(R) (2006).

³²D. A. Tenne *et al.*, Phys. Rev. B **71**, 132512 (2005).

³³K. A. Yates *et al.*, Phys. Rev. B **68**, 220512(R) (2003).

³⁴A. V. Pogrebnikov *et al.*, Phys. Rev. Lett. **93**, 147006 (2004).

³⁵M. Putti *et al.*, Phys. Rev. B **71**, 144505 (2005).

³⁶G. Campi *et al.*, Eur. Phys. J. B **52**, 15 (2006).

³⁷L. Boeri *et al.*, Phys. Rev. B **65**, 214501 (2002).